The University of Western Australia

The Use of Magnetometry Techniques to Characterise the Size Distribution of Magnetic Nanoparticles

by

Jason Heeris

Submitted in partial fulfilment of
the requirements for the degree of

Bachelor of Science (Honours)

School of Physics
The University of Western Australia

October, 2005

Contents

ABSTRACT

The Use of Magnetometry Techniques to Characterise the Size Distribution of Magnetic Nanoparticles

by Jason Heeris

Supervisors: *Dr. R. Woodward and Dr. T. G. St Pierre*

T he use of SQuID magnetometry to characterise the particle size distribution of magnetic nanoparticles was investigated using a variety of techniques and compared to results from transmission electron microscopy (TEM) and small angle neutron scattering (SANS). In particular, temperature dependent magnetic viscosity measurements were compared with other magnetometry techniques, and variations on typical experimental parameters were explored in order to gain a better picture of the size distribution and the effectiveness of various measurement techniques. Magnetic viscosity experiments on a sample of magnetite nanoparticles using an initial field of 100Oe were found to give a moment-weighted energy barrier distribution consistent with a log-normal distribution of particle diameters with a mean of 5.9nm and a standard deviation of 1.6nm, compared to values obtained from TEM of 3.7nm and 0.9nm, and SANS values of 3.2nm and 0.6nm.

Acknowledgements

To both of my supervisors, Robert Woodward and Tim St Pierre, I am deeply grateful for all of the advice, guidance, expertise and moral support – I could not have asked for better supervisors. I also owe a great thanks to David Crew who, because of knowledge and often just proximity, was often a *de facto* supervisor.

I am also indebted to the help and support of the staff at the UWA Centre for Microscopy and Microanalysis, especially Martin Saunders, Steve Parry and Nigel Smith, without whom I would likely still be trying to count blurry smudges on a blurrier background.

To Dave McPhee, thank you for your help and supply – often at short notice – of cryogenics essential for the temperature dependent experiments.

To Metha Rutnakornpituk, Thompson Mefford and Shane Thompson, who took the time to visit and brought with them valuable suggestions and support.

To Elliot Gilbert and Jamie Schulz, for all their help with the SANS experiments and data analysis.

Finally I would like to thank my fellow honours students, particularly Jane Turner.

Chapter 1

Introduction

There are a variety of methods by which the particle size distribution of magnetic nanoparticles may be measured – typical experimental techniques include direct imaging, bulk scattering and macroscopic magnetic measurements. While imaging methods such as transmission electron microscopy (TEM) provide clear visual evidence of the sizes of particles, only a limited number of particles can be analysed, it is often the case that sample preparation biases the observed distribution, and problems of resolution, contrast and analysis introduces ambiguities. Scattering techniques such as small angle neutron scattering (SANS) can be used to study large ensembles, but sensitivity of the scattering experiment to other elements introduces noise and uncertainty, and results are often biased by the models used in analysis.

Magnetometry allows for macroscopic measurements of a complete ensemble of particles. Interpreting these measurements and relating them to size distribution, however, is less direct than TEM and relies on models that are not always valid and experiments that may depart from underlying assumptions.

In this report techniques for determining information about particle size are investigated and compared. In particular, the use of magnetic viscosity measurements and variants of this experiment are used to produce a volume distribution which can be compared to that found from SANS and TEM imaging.

1.1 Motivation

Most applications of magnetic nanoparticles require particles to be produced with well defined, narrow size distributions. An accurate and reliable method of characterising the sizes of particles is of interest to those developing and improving manufacturing processes as well as those using them.

The use of magnetic nanoparticles for biomedical applications[22] also requires that the particles be biocompatible – leading to a particular interest in magnetite – and stable in suspension, which is achieved through a polymer coating[9, 13, 24, 29] of the particles. Knowledge of how these coatings inhibit aggregation in solution is vital to their develop-

ment, and so the sensitivity of magnetometry to close range particle interactions is also relevant to these applications.

Various methods for measuring particle size distributions have been explored and suggested by other authors – magnetic viscosity was used by Gorham to examine the energy barrier distribution in horse-spleen ferritin[11, 25] and by Barbara et al. on Ba-ferrite nanoparticles[2]; weak field relaxometry was used by Berkov and Kötitz on fine Ba-ferrite particles[6] and by Romanus et al. on iron oxide nanoparticles[23]; Hanson et al. estimated particle sizes from field cooled/zero field cooled experiments[12] and Lu et al. have suggested[18] one way of using these methods to look at the volume distribution.

1.2 Aims of This Study

Samples obtained from two different production techniques for magnetic nanoparticles were used to compare a series of methods for determining particle size and distribution characteristics. Magnetometry techniques will be compared with each other and to the more established methods of TEM and SANS to gauge the effectiveness and accuracy of magnetic measurements in determining the size distribution of magnetic nanoparticles. Of particular interest is the use of temperature dependent magnetic viscosity measurements to render a full picture of the distribution of energy barriers arising from particle volumes, and the effects of modifications of the experimental parameters to obtain a more accurate picture.

Chapter 2

Background

Several techniques of magnetometry will be investigated with a view to obtaining and comparing particle size distributions, including field cooled/zero field cooled measurements, hysteresis above and below the blocking temperature, magnetic viscosity and weak field relaxometry.

2.1 Superparamagnetism

In bulk magnetic materials, domains of magnetic order and the transitions between them may be up to hundreds of nanometres in size. In a particle with dimensions of the order of nanometres there is not enough room for multiple domain formation and a nanoparticle will exhibit magnetic behaviour different to that seen on larger scales.

Since a single crystal magnetic nanoparticle does not have sufficient size to support multiple magnetic domains, under an applied field the magnetisation must rotate to align with the field (Néel rotation). Crystalline materials usually have a single 'easy' axis along which the magnetisation prefers to lie, thus creating an energy barrier to the rotation of magnetisation. Such a situation is described by the Stoner-Wohlfarth model[26] which assumes an energy barrier E of the form

$$E = KV\left(1 - \frac{H}{H_A}\right)^2$$

K : the magnetocrystalline anisotropy constant
V : the volume of the particle
H : the applied field

and $H_A = 2K/\mu_0 M_S$ is the *anisotropy field* (or *activation field*) of the particles, ie. the field at which the energy barrier to magnetic reversal disappears.

When the thermal energy of the system becomes comparable to the size of this barrier, the particle will rapidly fluctuate between magnetisation states and appear to have zero net magnetisation – a phenomenon known as *superparamagnetism*. The temperature at

which this phenomenon occurs is called the *superparamagnetic blocking temperature*, T_B, and depends on the time for which the magnetisation is observed.

The magnetisation of a system of identical, ideal superparamagnetic particles above the blocking temperature is given by the Langevin function[19]:

$$\begin{aligned} M(B) &= M_0 \mathcal{L}\left(\frac{mB}{kT}\right) \\ \text{where} \qquad \mathcal{L}(x) &= \coth(x) - \frac{1}{x} \end{aligned}$$

M_0 : the saturation magnetisation
m : the (weighted average) moment per particle
B : the magnetic field
T : the temperature of the system

The parameter m can be used to estimate the average size of the particles if the moment per unit cell of the material is known.

This model does not account for anisotropy or distributions of particle sizes, and so deviations from this behaviour should be expected in samples with broad distributions of these properties.

2.2 Experimental Methods

2.2.1 Field Cooled/Zero Field Cooled Experiments

Field cooled/zero field cooled (FC/ZFC) measurements consist of two parts: cooling the sample from above the blocking temperature to low temperatures (2–5K) in a saturating field and measuring the magnetic moment in some small field – smaller than the anisotropy field – at incremented temperatures. This is then repeated after cooling in zero field. As the temperature is raised after cooling in a field, the saturated particles will unblock (become superparamagnetic) – if there is a distribution of blocking temperatures in the system, this will appear as a gradual decrease in magnetisation. After cooling in zero field the system should have no net magnetisation, but until the particles begin to unblock they will not respond to the probe field. As the largest fraction of particles unblock a peak is seen in the zero field cooled curve, and as the remainder unblock the curve meets that of the field cooled magnetisation (Fig. 2.1).

The data can be used to identify the maximum blocking temperature T_B for the particles in the ensemble (see Fig. 2.1), which is used to specify the temperature range used for magnetic relaxometry experiments, and can be used to estimate the maximum particle size from

$$E = KV$$

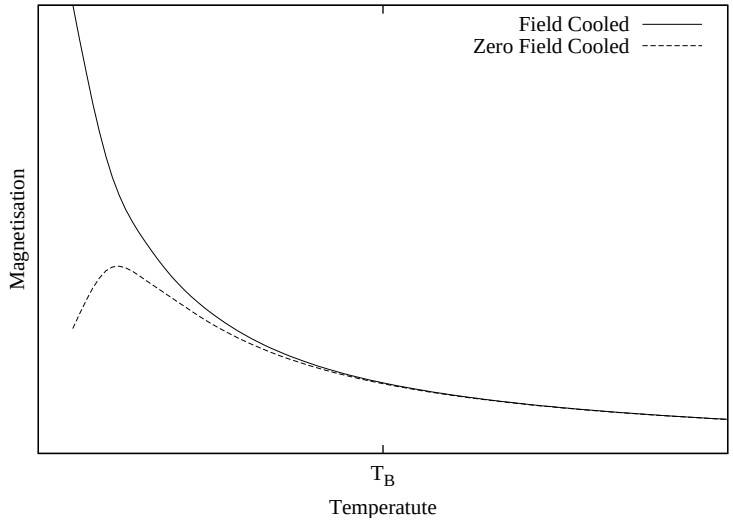

Figure 2.1: *An example of a FC/ZFC curve, showing the blocking temperature where the two curves meet*

$$\begin{aligned} \text{and } \tau_N &= \tau_0 e^{E/kT} \approx t_m \\ \text{so } a \approx \frac{6V}{\pi}^{1/3} &= \left(\frac{6kT}{\pi K} \ln\left(\frac{t_m}{\tau_0}\right)\right)^{1/3} \end{aligned} \tag{2.1}$$

τ_N : the Neèl relaxation time
K : the magnetocrystalline anisotropy constant
V : the volume of the particle
a : the diameter of the particle
t_m : the measurement time
τ_0 : a material specific time constant ($\sim 10^{-9}$s)
T : the temperature

Lu et al[18] have suggested that the derivative of the difference between the two curves gives the distribution of blocking temperatures. This method essentially looks at the fraction of particles that make the transition from blocked to unblocked as the temperature is incremented. This can be related to the *moment-weighted energy barrier distribution* $q(E)$:

$$q(E) = \frac{\Delta\left((m_{ZFC} - m_{FC})\right)}{\Delta T} \tag{2.2}$$

$q(E)$: the moment-weighted energy barrier distribution
$m_{FC(ZFC)}$: the field cooled (zero field cooled) moment
T : the temperature

The moment-weighted energy barrier distribution is discussed in greater detail below, and Eq. 2.10 shows how it can be used to find the size distribution of particles.

2.2.2 Magnetic Viscosity and Weak Field Relaxation

The magnetic relaxation behaviour of an ensemble of magnetic entities depends on the energy barriers that are present in the system. In a system consisting of many magnetic entities each with an energy barrier E, an individual particle will relax from the metastable state into the stable state with a characteristic time constant

$$\tau_N = \tau_0 e^{E/kT}$$

τ_N : the Neèl relaxation time
τ_0 : a material specific time constant ($\sim 10^{-9}$s)
E : the energy barrier of the particle
T : the temperature of the system

The actual time taken for any given particle to relax is distributed randomly by the exponential distribution e^{t/τ_N} with characteristic time τ_N. Any particles with τ_N significantly less than the measurement time are superparamagnetic and do not contribute to the measured moment in zero field.

Magnetic viscosity and weak-field relaxometry are two different experiments that measure this magnetic relaxation, and the resulting data can be converted to a moment-weighted distribution of the energy barriers in the system. In magnetic viscosity measurements the system starts from a saturated state, and in the case that the energy barrier distribution is broad, decays by[27]:

$$m(t) = m_0 - S \ln\left(\frac{t - t_0}{\tau}\right) \tag{2.3}$$

$m(t)$: magnetic moment at time t
S : the coefficient of magnetic viscosity
t_0 : starting time of the measurement
τ : an arbitrary scaling factor (usually taken as 1s)
m_0 : an offset moment

The fit parameter m_0 is dependent on the value chosen for the scaling factor τ; while a better (ie. more independent) fit parameter might be $e^{S/m}$, in practice this quantity varies far too quickly for proper fitting. It is the fit parameter S in Eq. 2.3 in which we are interested, since it is related to $q(E)$, the moment-weighted energy barrier distribution[27, 11]:

$$\begin{aligned} S &= kTq(E_c) \\ \text{where} \quad E_c &= kT \ln\left(t_m/\tau_0\right) \end{aligned} \tag{2.4}$$

E_c : the energy of the barriers being observed
$q(E_c)$: the moment-weighted energy barrier distribution

Because the system starts from a saturated state all energy barriers have been activated, and during the time of the measurement we observe the relaxation only over energy barriers close to E_c, provided that the energy barrier distribution is wide compared to kT.

Weak field relaxometry starts by perturbing the system with a small field. After the field is removed, the subsequent relaxation should follow[6]:

$$m(t) = A \ln\left(\frac{t_H}{t - t_0} + 1\right) + m_0 \tag{2.5}$$

$m(t)$: magnetic moment at time t
A : the relaxation parameter
t_0 : starting time of the measurement
t_H : an effective magnetising time
m_0 : an offset moment

This experiment is constrained to situations in which the magnetising field is small, such that:

$$H \ll H_A / \ln(t_H/\tau_0)$$

The parameter A relates to the energy barrier distribution in the same way as S:

$$A = kTq(E_c) \tag{2.6}$$

The fundamental difference between these experiments is that a magnetic viscosity experiment begins with all particles in one metastable energy state and observes the relaxation only of particles with energy barriers near the thermal energy. The assumption that the distribution of energy barriers in the system is broad compared to the thermal energy means that over the course of the experiment a relatively small number of particles will reverse, and the number returning to the saturated state is negligible.

Weak field relaxometry, on the other hand, relies on perturbing just a fraction of particles from the equilibrium state and observing the thermalisation of all of these activated particles. The assumption is that the perturbation is small compared to the energy barrier so that the system remains close to equilibrium, and population changes in both directions are significant.

Both experiments should yield the same information – the moment-weighted energy barrier distribution $q(E)$ – and in the next section we see how to derive the particle size distribution from $q(E)$.

2.3 Magnetorelaxometry and Particle Size Distribution

To analyse the relationship between the distribution of volumes of the particles and the energy barrier distribution of the system, consider an ensemble of magnetic entities with energy barriers E and volumes V. If it is assumed that the energy barrier of a single particle is related only to its volume – ie. $E \equiv E(V)$, then it can be shown that (Appendix A):

$$\rho_V(V) = \rho_{E,V}(E)\,\frac{dE}{dV} \tag{2.7}$$

$\rho_{E,V}(E)$: the energy barrier distribution arising from particle volumes
$\rho_V(V)$: the volume distribution

Because particles with a larger change in moment contribute more to the measured response, the quantity measured in viscosity experiments is the *moment weighted* energy barrier distribution:

$$q(E) = \rho_{E,V}(E)\,m_V(E). \tag{2.8}$$

where $m(E)$ is the change in magnetic moment associated with reversal over the energy barrier E.

Combining Eqs. 2.8 and 2.7, we have

$$\rho_V(V) = \frac{dE}{dV}\,(m_V(E))^{-1} q(E). \tag{2.9}$$

Considering an ensemble of magnetic nanoparticles, we make the following assumptions:

1. The particles can be modelled by the Stoner-Wohlfarth model[26] with energy barrier $E = KV$, where K is the crystalline anisotropy constant

2. The volume of the nanoparticle is the volume of its associated magnetic entity

3. The values of the anisotropy constant and saturation magnetisation for a bulk material can be used for the nanoparticle

4. The angles of the easy axes of the particles are isotropically distributed.

Implicit in the first assumption is that surface and shape effects may be ignored for the particles. However, for particle sizes of the order of 5nm a significant fraction of the atoms are at the surface of the particle, and so surface anisotropy could conceivably become a dominant factor. If, however, the particles are roughly spherical then these surface effects should cancel out to a large extent and any shape or surface anisotropy should be negligible.

From assumption 1, $dE/dV = K$. From assumptions 2, 3 and 4, we have $m_V(E) = M_S V$ (for M_S the saturation magnetisation). Equation 2.9 then becomes:

$$\rho_V(V) = \frac{K}{VM_S} q(KV).$$

In an identical way we can relate $q(E)$ to the distribution of particle diameters by combining the analogy of Eq. 2.9 with the assumption that the particles are roughly spherical, so $V \approx \pi a^3/6$ (where a is the diameter of a particle). The energy barrier is then $E = \pi K a^3/6$, which gives:

$$\rho_a(a) = \frac{3K}{M_S a}\, q\left(\frac{\pi K a^3}{6}\right) \tag{2.10}$$

It may well be the case that our assumption above – that E depends only on V – does not apply to a sample of nanoparticles where there may be a relative dominance of surface effects or interparticle interactions to account for. In the case where there are different, *independent* physical origins for the energy barriers in a system, the moment weighted energy barrier distribution is a sum over the separate physical systems:

$$q(E) = \sum_i \rho_{E,i}(E)\, m_i(E)$$

This would be the case if an additional component arose from a spin glass phase at the surface of the particle[15, 11] or from 'spin canting' at the surface or at lattice defects in the particle[20]. If, however, it is due to a distribution of anisotropy fields or to particle interactions then $q(E)$ becomes a convolution of these distributions[2] and the volume component is more difficult to extract.

For example, while the volume distribution is usually log-normal, it has been found that there can also be an exponential component to the energy barrier distribution[11, 25] of magnetic nanoparticles. If we assume that all particles are spherical, then a log-normal volume distribution implies that particle diameters also follow a log-normal distribution. The diameter distribution gives rise to one component of $q(E)$:

$$\begin{aligned} \rho_a(a) &= \frac{q_1'}{aS_1'\sqrt{2\pi}} \exp\left(-\left(\frac{\ln(a/M_1')}{\sqrt{2}S_1'}\right)^2\right) \\ \Rightarrow q_V(E) &= \frac{q_1}{S_1\sqrt{2\pi}} \exp\left(-\left(\frac{\ln(E/M_1)}{\sqrt{2}S_1}\right)^2\right) \end{aligned} \tag{2.11}$$

where:

$$\begin{aligned} q_1 &\equiv \frac{K}{M_s} q_1' \\ S_1 &\equiv 3S_1' \end{aligned}$$

$$M_1 \equiv \frac{M_1'^3 K\pi}{6}$$

The total moment-weighted energy barrier distribution becomes the sum of that arising from the volume distribution and any additional distributions:

$$\begin{aligned} q(E) &= q_V(E) + q_{exp}(E) \\ &= \frac{q_1}{S_1\sqrt{2\pi}} \exp\left(-\left(\frac{\ln(E/M_1)}{\sqrt{2}S_1}\right)^2\right) + q_2 \exp(-E/M_2) \end{aligned} \tag{2.12}$$

For the purposes of identifying the features of the volume distribution, it may be adequate to simply account for this behaviour rather than explain the physical source of it, which is beyond the scope of this report.

Chapter 3

Materials and Methods

Two samples of magnetic nanoparticles manufactured using different methods were examined in this work.

3.1 Nanoparticle Samples

Two samples of nanoparticles in suspension were supplied by collaborators at the Virginia Polytechnic Institute and State University in the USA and at Naresuan University in Thailand. The first (designated MR), a sample of magnetite coated in oleic acid dispersed in hexane (C_6H_{14}), was made by high temperature decomposition of $Fe(acac)_3$ using the La Mer process, where the concentration of reagents is raised above the critical point for nucleation for a very short time in order to control the size of particles.

The second (designated LH) is a sample of magnetite particles coated in a triblock copolymer suspended in H_2O, manufactured by a constrained geometry, or reverse micelle, method where the particles are grown inside hydrophilic pores of a polymer jacket which control the size of the particles. These two methods are illustrated in Fig. 3.1.

3.2 SQuID Magnetometry

All magnetometry was performed on a Quantum Design Magnetic Properties Measurement System (MPMS-7) employing a superconducting quantum interference device (SQuID) sensor. The temperature of the sample chamber can be set between 2—700K and the applied field can be set up to 70kOe in either direction along the vertical axis. Experiments performed on the SQuID-MPMS included field cooled/zero field cooled measurements, hysteresis measurements and various magnetic relaxometry experiments which were discussed in detail in Cha. 2.

One sample for magnetometry was made from each stock of suspended nanoparticles by placing a small amount ($\sim$1mL) in a sample container. Sample MR02 was made from the oleic acid coated particles and contains 3.8μg of magnetite, and LH01 was made from

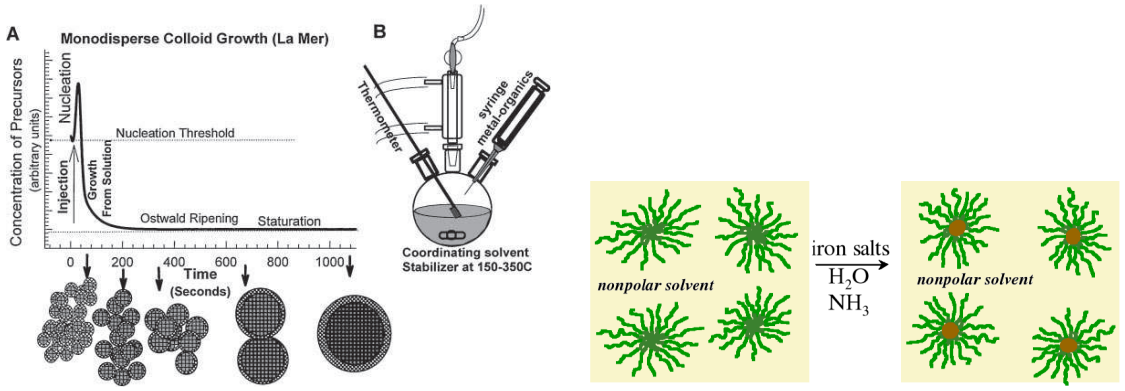

(a) Schematic of the La Mer process illustrating control of nucleation and growth (left) and a typical apparatus (right). From Murray et al.[21]

(b) The constrained geometry method grows the particles inside polymer jackets[13]

Figure 3.1: *Two processes used for the manufacture of nanoparticles*

the triblock copolymer stock and contains 1.0μg of magnetite (weights determined from hysteresis measurements).

In a sample of dried nanoparticles it may not be reasonable to neglect interparticle interactions, as the particles would be separated only by their polymer coating. In an attempt to investigate the effects of particle separation, a sample was made (designated MR03) consisting of nanoparticles suspended in PDMS – a polymer that can be made to solidify under application of intense ultraviolet light. The dilution of the particles and their stability in suspension in the solvent and polymer should greatly increase the separation of the particles in the PDMS.

3.3 Transmission Electron Microscopy

Transmission electron microscopy was performed on a sample from the MR stock solution using the JEOL 3000-FEG. Limited information about shape and structure could be determined, and some idea of particle size distribution was determined. The JEOL 3000-FEG uses a field emission gun coherent electron source and an accelerating voltage of 300kV, both of which allow for greater resolution but cause a decrease in contrast.

Samples for TEM were made from the MR stock solution by successive dilutions of about 1 : 20. Suspensions of nanoparticles were pipetted onto 3mm copper grids coated with a 40nm carbon substrate which were allowed to dry. Dilutions were required as a sample that is too concentrated will show stacking of particles and will not be useful for particle size measurements, but a sample that is too dilute will make it difficult to find particles to image. It was found that the use of distilled solvents to suspend and dilute the particles was essential, as contamination with polymers, releasing agents and other contaminants will significantly decrease the contrast and resolution of the images.

3.4 Small Angle Neutron Scattering

Small angle neutron scattering was performed at the AUSANS Facility adjoining HIFAR at the Australian Nuclear Science and Technology Organisation (ANSTO)[28]. The neutron flux at the sample is of the order of $10^4 \mathrm{n\,cm^{-2}\,s^{-1}}$ and the operational range of Q, the scattering vector, is 0.01–0.1Å. A sample was prepared using the MR stock solution, allowing the hexane to evaporate, and re-dispersing the particles in completely deuterated cyclohexane (C_6D_6). The use of deuterated solvents significantly reduces noise from inelastic scattering of the neutrons that is associated with protons in protonated solvents.

The SANS data was analysed using *Irena*, a package of small angle scattering data analysis macros for the Igor Pro data processing software. *Irena* uses the models outlined by Beaucage et al.[3, 4, 5] and allows for the combination of different distributions of scattering entities with various geometries and scattering contrasts, and can incorporate structure arising from interactions between particles.

Chapter 4

Results and Discussion

The outcomes of each of the magnetometry techniques employed, and the results of TEM and SANS, are detailed and compared here. Each method provides a different insight into the nature of the two samples provided and ultimately a picture is constructed of the size distribution of the particles and the capabilities and limitations of each experiment.

Analysis of magnetometry makes use of the following bulk values for the properties of magnetite, taken from Cullity[10], except μ/μ_B and M_A from Chikazumi[8]:

M_0	0.510	$\mathrm{MA\,m^{-1}}$	Saturation magnetisation at 0K
σ_0	98	$\mathrm{J\,kg^{-1}T^{-1}}$	Specific saturation magnetisation at 0K
M_s	0.480	$\mathrm{MA\,m^{-1}}$	Saturation magnetisation at 293K
K	-1.1×10^4	$\mathrm{J\,m^{-3}}$	Crystal anisotropy constant
ρ	5.24×10^3	$\mathrm{kg\,m^{-3}}$	Density
μ/μ_B	4.1		Moment per unit cell
M_A	231.55		Molecular weight

4.1 SQuID Magnetometry

4.1.1 Hysteresis

Hysteresis loops for each sample were measured at 300K, 5K and 2K. Figure 4.1 shows the data for MR02 taken at 2K and corrected for a linear component at high field. The essential features of all other curves are summarised in Tab. 4.1. The 0K magnetisation of magnetite was used to find a scaling factor to convert between magnetisation and moment for each sample by $M = \xi m$.

It was observed that the hysteresis loop at lower temperatures remained open up to large fields. This indicates the presence of large barriers to reversal – most likely due to a tail in the distribution of anisotropies in the particles arising from surface anisotropy, casting some doubt on the assumptions made in Sec. 2.3 regarding surface effects.

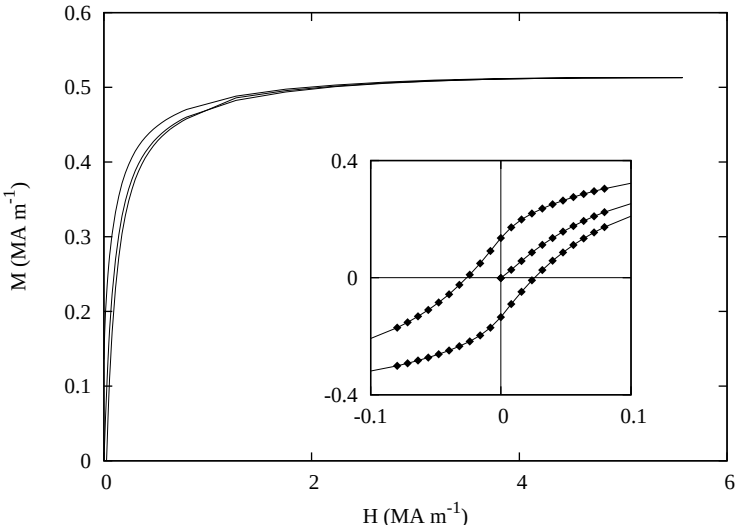

Figure 4.1: *Hysteresis of MR02 at 2K, corrected for linear component. Inset shows detail near zero field.*

Table 4.1: *Summary of properties found from hysteresis measurements*

Sample	Temp (K)	Major Phase	χ_{HF} (10^{-3})	χ_{LF}	H_C ($10^4\,\mathrm{Am}^{-1}$)	m_s ($10^{-4}\,\mathrm{JT}^{-1}$)	M_R ($10^5\,\mathrm{Am}^{-1}$)	Moment scaling factor $\xi \equiv M_s/m_s$ ($10^9\mathrm{m}^{-3}$)
MR02	2	FM	9.76	-	2.60	3.70	1.35	1.515
	5	FM	10.2	-	0.647	3.68	0.58	
	300	SPM	-	0.473	-	-	-	
MR03	2	FM	-81.6	-	4.54	0.0503	3.69	101.5
	5	FM	-76.5	-	0.824	0.0313	1.81	
	300	?	-	0.230	-	-	-	
LH01	2	FM	-1.23	-	1.96	1.01	1.27	5.547
	5	FM	-1.74	-	1.74	1.07	1.17	
	300	SPM	-	3.85	-	-	-	

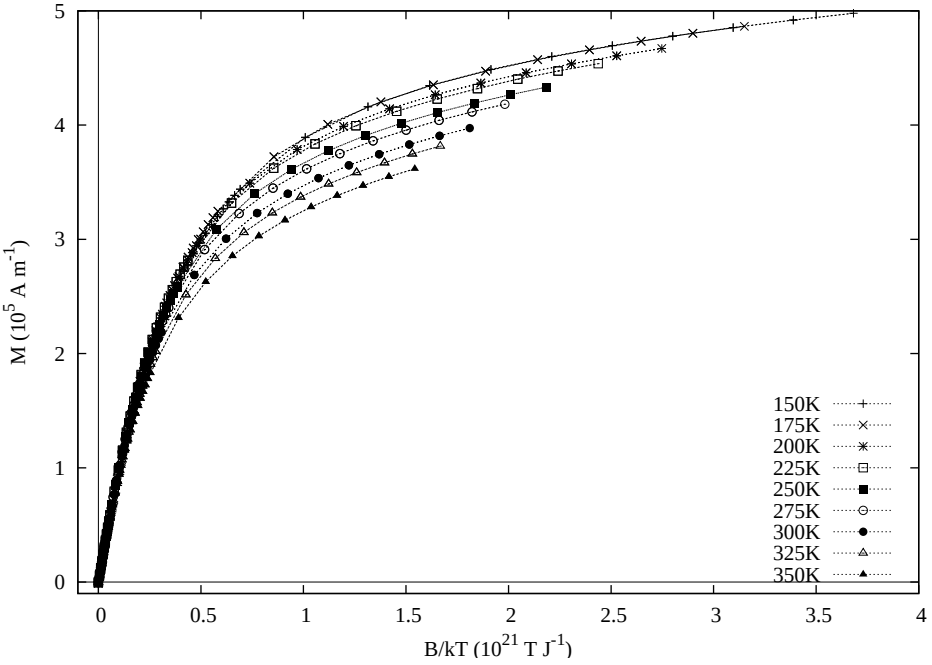

Figure 4.2: *M vs B/kT for MR02*

4.1.2 Temperature Dependence of Superparamagnetism

The superparamagnetic behaviour of MR02 and LH01 was investigated by taking hysteresis measurements at temperatures above the blocking temperature. If the nanoparticles behaved as ideal superparamagnetic particles then plotting M against B/kT should show the data lying along a single curve. Figure 4.2 shows the data obtained for temperatures between 150—350K for MR02, which clearly does not conform to this behaviour; this is expected as the Langevin model does not account for the anisotropy of the particles or for a distribution of particle sizes[14, 19].

At each temperature, the data were fitted to the equation:

$$M(B) = Nm\mathcal{L}\left(\frac{mB}{kT}\right) + \epsilon B$$

... where N is constrained to be constant across all temperatures but m is allowed to vary. The linear component was required to significantly improve the fit for both samples, and may arise from contamination by para- or diamagnetic material, or a distinct magnetic phase in the particles themselves. If the linear behaviour does correspond to some physical magnetic phase, then the parameter ϵ relates to the susceptibility χ by

$$\epsilon = \mu_0^{-1}\frac{\chi}{1+\chi}$$

Figures 4.3 and 4.4 show the fit values obtained for MR02 and LH01. The values of χ for both samples could be fitted quite well to a Curie-Weiss law $\chi = D + \frac{C}{T-\theta}$, but the values obtained did not represent physically realistic magnetic behaviour and it is doubtful

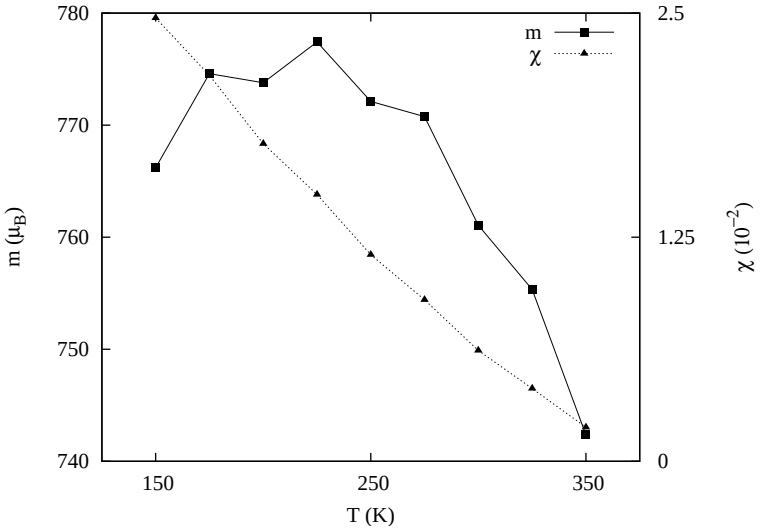

Figure 4.3: *Langevin fit parameters for MR02*

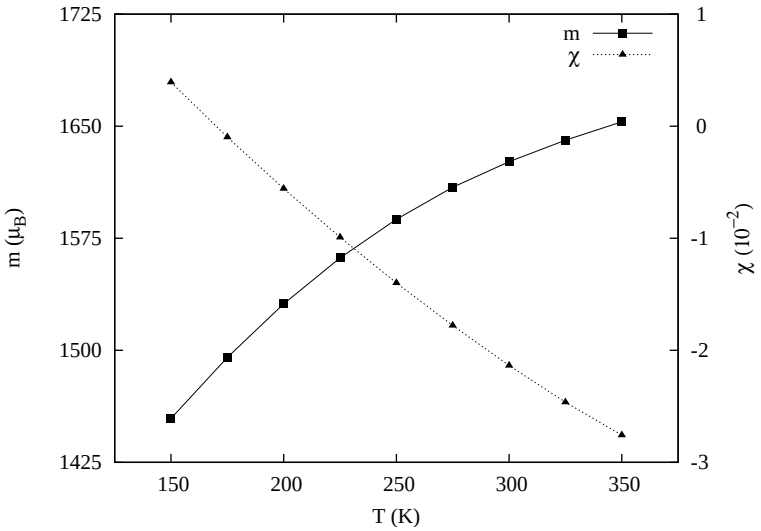

Figure 4.4: *Langevin fit parameters for LH01*

Table 4.2: *Particle sizes found from the fit parameter m*

Sample	Mean Diameter (nm)
MR02	2.94–2.98
LH01	3.67–3.83

that this linear component arises from a physical magnetic phase. In particular, the value of θ was found to be negative indicating antiferromagnetic behaviour, but was greater than the range of temperatures used. It therefore cannot be due to an antiferromagnetic phase as the susceptibility should decrease with decreasing temperature below the Neèl temperature for an antiferromagnet.

The values found for m were used to estimate the mean size of particles by comparing to the magnetic moment of the unit cell of magnetite (see Tab. 4.2).

The fact that m increases for LH01 is contrary to the expected behaviour, and this together with the non-physical behaviour of χ reflects the fact that we are fitting to a model that does not adequately describe a system containing a broad distribution of particle sizes and anisotropies.

4.1.3 Field Cooled/Zero Field Cooled Measurements

Field cooled/zero field cooled measurements were performed on samples MR02 and LH01 using a saturating field of 70kOe and a probe field of 50Oe. Table 4.3 shows blocking temperatures and estimated maximum particle sizes obtained from Eq. 2.1.

Table 4.3: *Maximum particle sizes as estimated from FC/ZFC measurements*

Sample	Blocking Temp.	Max. Particle Diameter
MR02	50K	13nm
LH01	150K	19nm

The method suggested by Lu et al.[18] was used to find the moment-weighted energy barrier distribution, which was then converted to the size distribution shown in Fig. 4.5 using Eq. 2.10. The mean and standard deviation of this distribution are 5.5nm and 1.3nm. The prominent scatter of the data is possibly due to the variable thermal overshooting in the MPMS-SQuID as it changes the temperature before each measurement. The detail shown is taken at temperatures below about 15K – this is discussed in Cha. 5.

4.1.4 Magnetic Viscosity

Magnetic viscosity experiments were performed on MR02 and LH01 using the established method of cooling in a saturating field, as well as various other experimental parameters

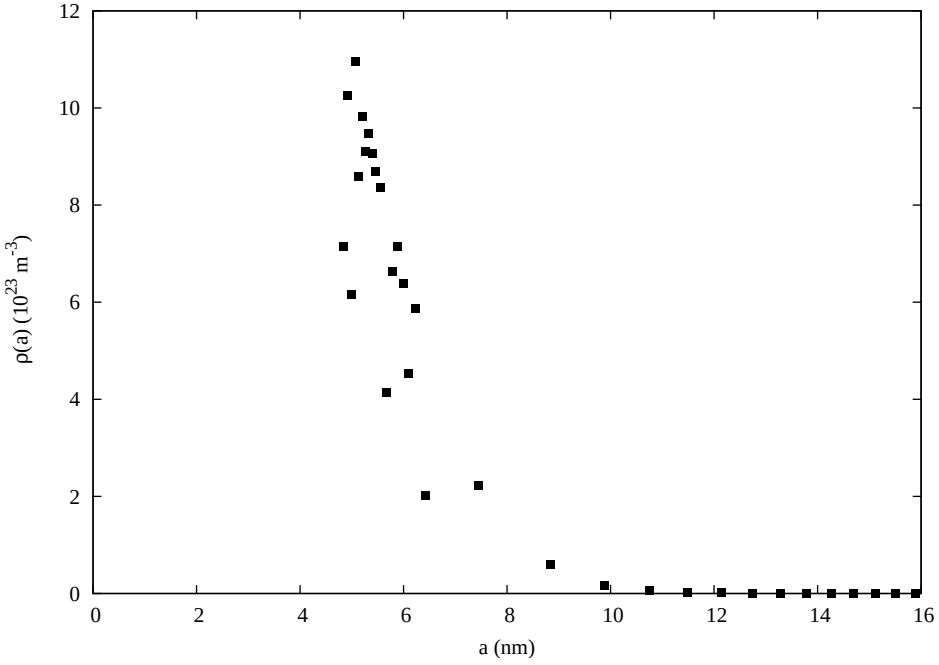

Figure 4.5: *Size distribution for MR02 obtained from FC/ZFC data*

to reduce components that obscure information about the particle size distribution.

For each temperature the samples were demagnetised by being raised above their blocking temperature and were then cooled in a 70kOe field. The field was removed when the temperature became stable and the decay of remanent magnetisation was measured over approximately 1000s. The resulting data are fitted by Eq. 2.3 for each temperature. The parameters S, m_0 and t_0 are found using the Levenberg-Marquardt non-linear regression algorithm with τ set to 1s. The viscosity parameter S is plotted against temperature for MR02 in Fig. 4.6.

The moment-weighted energy barrier distribution $q(E) = S/kT$ was calculated from the viscosity data for each sample. Temperature was converted to energy using $E = CkT$, where $C = \ln\left(\frac{t_{end}-t_0}{\tau_0}\right)$ with $\tau_0 = 10^{-9}$s[17]. It should be noted that while the ambiguity associated with τ_0 introduces some error, the scaling parameter C is insensitive changes in τ_0 because of the logarithmic dependence. Attempts to fit the distribution with the two component form of $q(E)$ (Eq. 2.12) were unsuccessful, but fitting to a pure exponential produced patterned residuals indicating an incomplete fit.

The uncertainty indicated in all viscosity plots is the statistical uncertainty (the asymptotic standard error) of the fitting procedure at that point. This is discussed in Sec. 4.1.6.

The Effect of Initial Field on Magnetic Viscosity

It has been found that using a lower priming field for viscosity measurements can decrease the diverging component of the energy barrier distribution[11]. This effect was investigated by performing additional viscosity measurements with priming fields of 5kOe, 1kOe

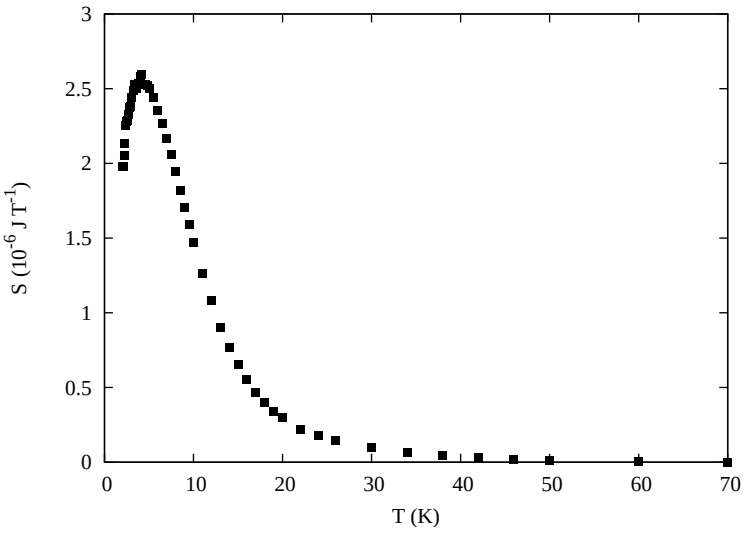

Figure 4.6: *Viscosity data for MR02 using an initial field of 70kOe*

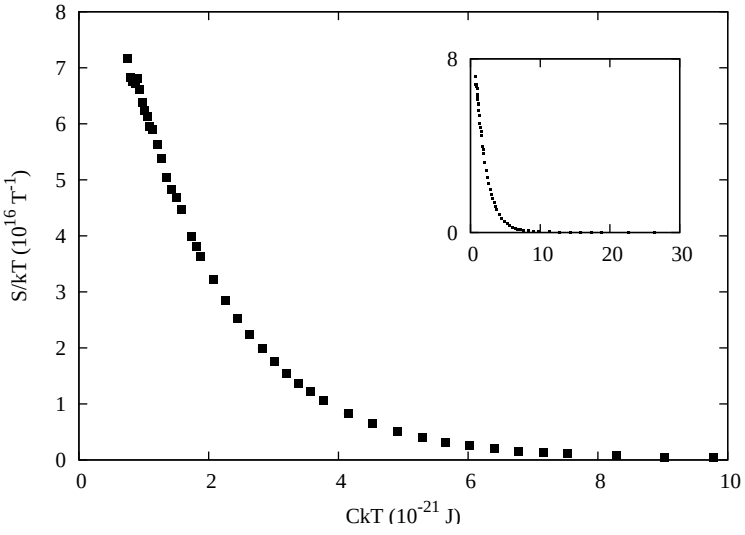

Figure 4.7: *Moment weighted energy barrier distribution for MR02 obtained from viscosity measurements using an initial field of 70kOe. Inset shows expanded energy axis.*

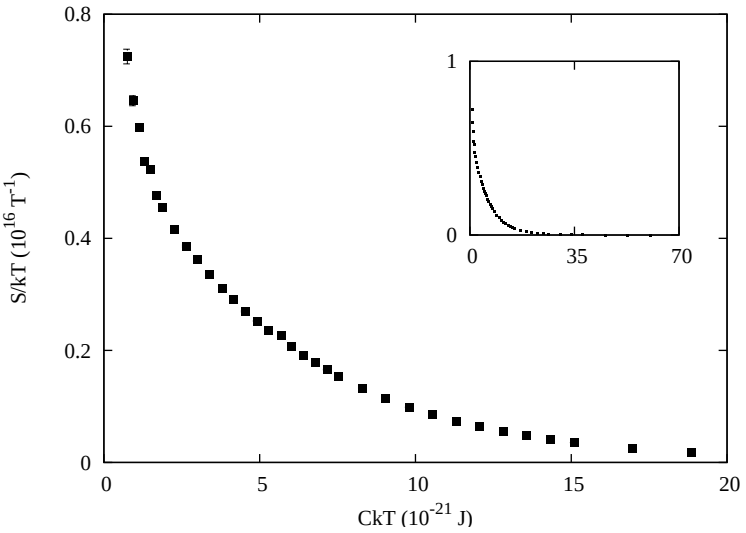

Figure 4.8: *Moment weighted energy barrier distribution for LH01 obtained from viscosity measurements using an initial field of 70kOe. Inset shows expanded energy axis.*

Table 4.4: *Log-normal particle size distribution properties from 100Oe viscosity experiments*

Sample	Mean (nm)	Mode (nm)	Std. Dev. (nm)
MR02	5.92	5.35	1.57
LH01	10.5	9.86	2.22

and 100Oe. The resulting energy barrier distributions are shown (with the original) in Fig. 4.9.

The distributions for 5kOe and 1kOe could not be properly fitted with either the two component or exponential form of $q(E)$, as with the 70kOe data. The distribution found from the 100Oe experiment, however, was fitted with the two-component form of $q(E)$ given in Eq. 2.12 and with the single volume component. Comparison of the standard deviation of the residuals showed that the two component fit is not a statistically significantly better fit. The fit parameters for $q_V(E)$ (see Eq. 2.11) were $q_1 = 4.23 \times 10^{16}\mathrm{J\,T^{-1}}$, $M_1 = 1.08 \times 10^{-21}\mathrm{J}$ and $S_1 = 0.782$, and the data and the single component fit are shown in Fig. 4.10.

A low priming field viscosity experiment was also performed on LH01 with a field of 100Oe. The resulting energy barrier distribution appeared to have both a log-normal component and an exponential component, and was fitted with the two component $q(E)$ (see Eq. 2.12). The calculated fit parameters were $q_1 = 1.07 \times 10^{15}\mathrm{J\,T^{-1}}$, $M_1 = 6.29 \times 10^{-21}\mathrm{J}$, $S1 = 0.627$,$q_2 = 8.20 \times 10^{14}\mathrm{J\,T^{-1}}$ and $M_2 = 5.15 \times 10^{-21}\mathrm{J}$.

Comparing these fit parameters to the form of the diameter distribution gives the statistical properties of the diameter distribution for each sample, summarized in Tab. 4.4 and plotted in Fig. 4.11.

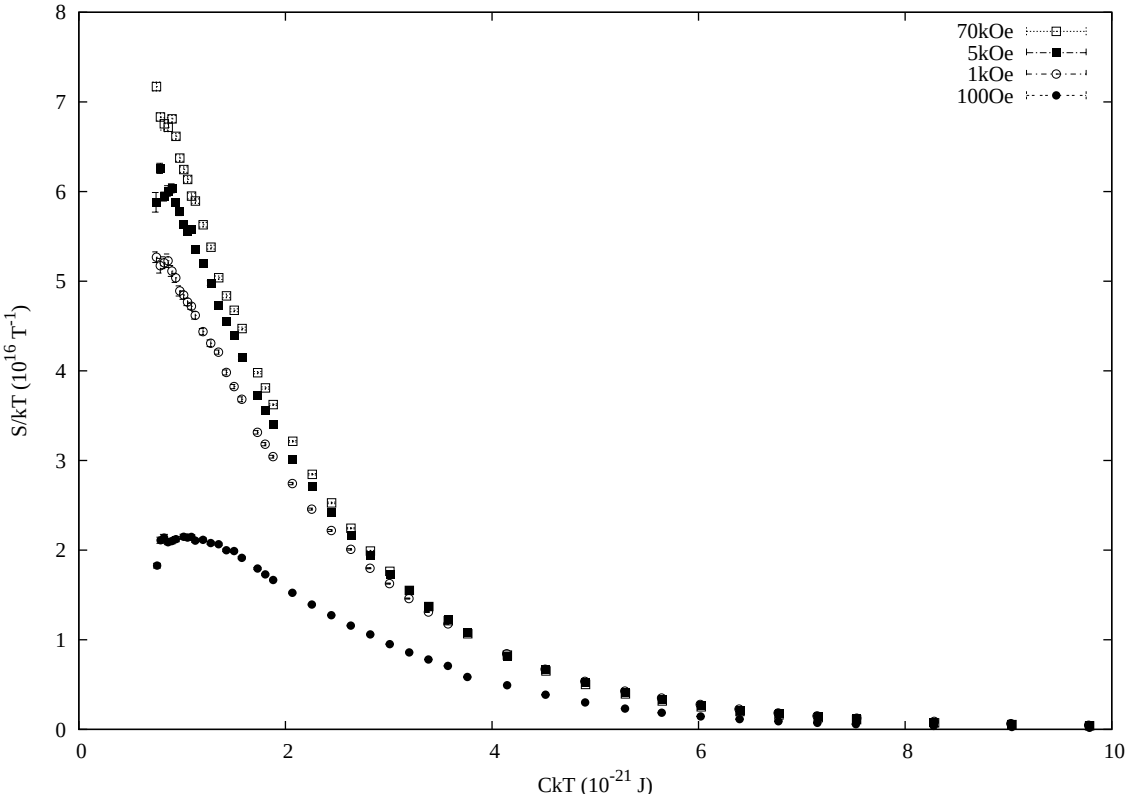

Figure 4.9: *Moment-weighted energy barrier distributions for MR02 calculated from viscosity data measured with different priming fields*

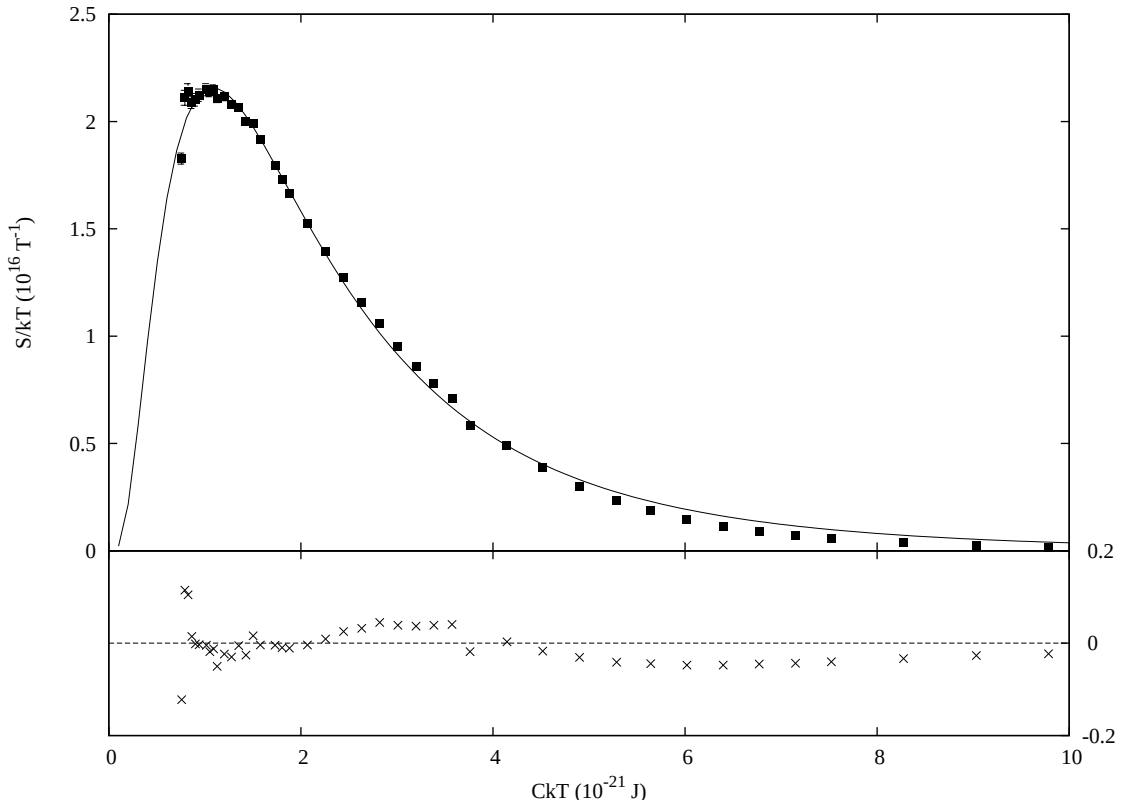

Figure 4.10: *Single component fit to the moment-weighted energy barrier distribution for MR02 found from 100Oe viscosity measurements (with residuals, lower)*

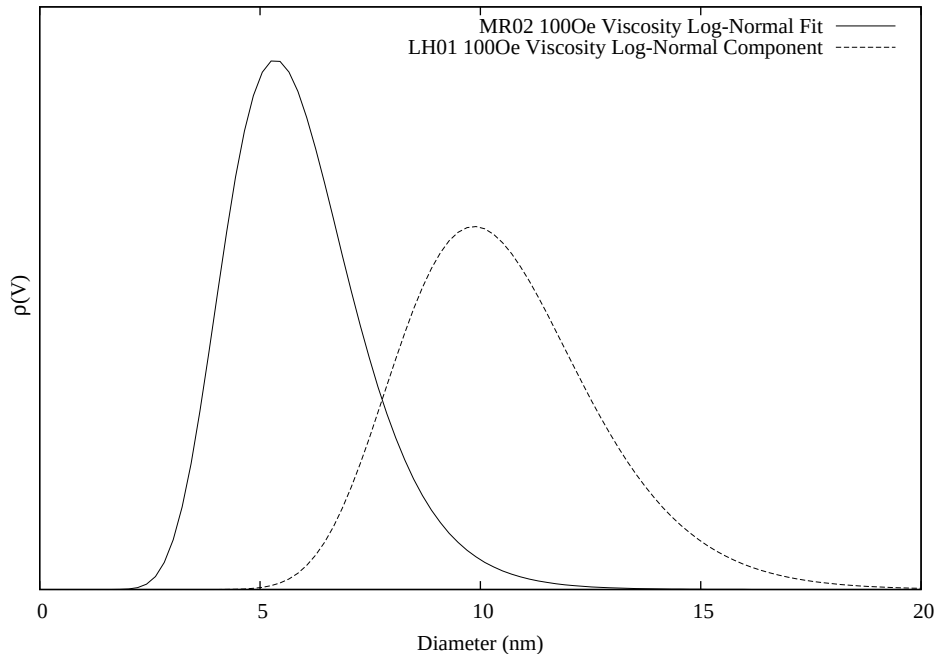

Figure 4.11: *Comparison of the fitted distributions to MR02 and LH01 found from 100Oe viscosity measurements*

The Effect of Particle Spacing on Magnetic Viscosity

One possible explanation for the exponential component in the energy barrier distribution is that it is related to interactions between nearby particles. The sample MR03 was made specifically to explore the effect of diluting and immobilising the particles to increase the distance between them. Viscosity measurements were performed to produce the moment-weighted energy barrier distribution shown with those of MR02 in Fig. 4.12.

The shape of the distribution for the PDMS sample does not show much change from that of the 70kOe viscosity data. It is difficult to make inferences from this about interparticle interactions, however, as it is possible that the particles form aggregates in the suspension; it is clear, though, that this method of sample preparation did not serve to reduce the unwanted component in the energy barrier distribution.

4.1.5 Weak Field Relaxometry

Weak field relaxometry follows a similar experimental procedure to magnetic viscosity measurements, but the sample is cooled in zero field with a small field applied after the temperature stabilises. In order to adequately fit the data it is necessary to measure at least one decade beyond the time for which the field is applied, ie. $t_{meas} > 10t_H$ and to apply a field for a period of time significantly longer than the time taken for the SQuID-MPMS to remove the applied field, which is between 30–60s. A further constraint on experimental parameters is that the strength of the field applied must be small: $H \ll H_A/\ln(t_H/\tau_0)$.

One weak-field relaxometry experiment was performed with a 1Oe field applied for

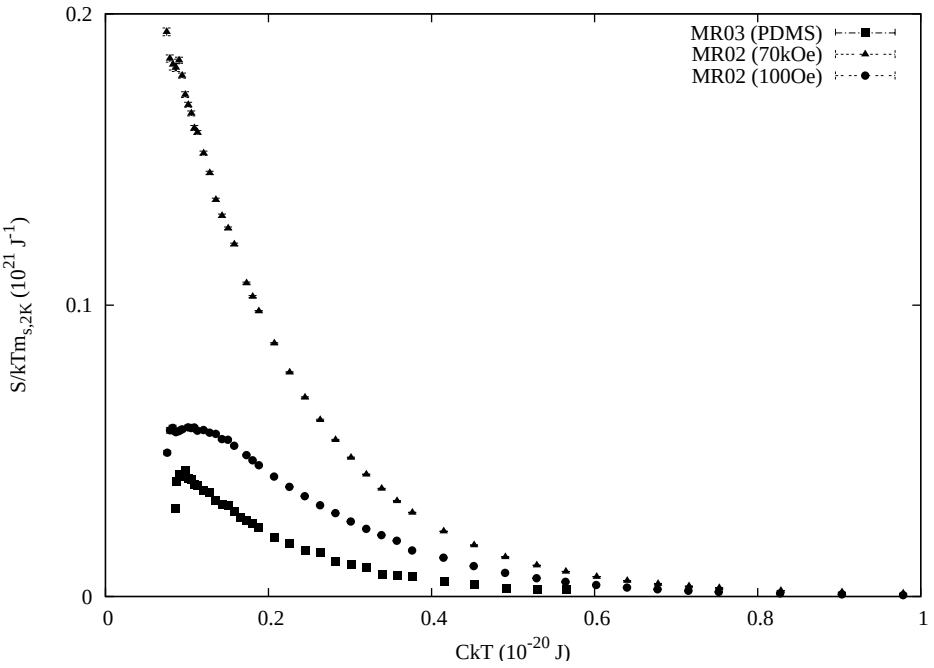

Figure 4.12: *Moment-weighted energy barrier distribution from viscosity measurements of MR03 (PDMS sample) compared with those of MR02 taken with 70kOe and 100Oe initial field*

300s and measurements over 6000s, using the same temperatures as for the viscosity measurements. Limitations of the SQuID-MPMS in measuring very weak moments made fitting the data difficult, but the nature of the function itself makes non-linear regression inherently unreliable – the uncertainty from the fitting procedure alone was greater than 100% at some temperatures, and some could not be fitted at all. The moment-weighted energy barrier distribution obtained from this experiment is shown in Fig. 4.13 and is obviously unsatisfactory.

4.1.6 Uncertainty

The moment measured by the SQuID-MPMS potentially has a systematic uncertainty of up to approximately 5% due to sample geometry. However, over the course of these measurements it is unlikely that this systematic offset changed by more than 1%. Since this consistently affects only the vertical scale of the results presented it has little effect on the determination of particle sizes, as that depends only on scaling along the temperature axis. The only measurements for which we are concerned with the actual value of the moment are the hysteresis measurements, as they are used to determine the weight of magnetite in the samples.

The processing of the data involved removing any data sets showing temperature drift of more than a few percent, so the statistical uncertainty in any temperature value is negligible. While technically this is the temperature set by the SQuID-MPMS and not the measured temperature of the sample, the fact that no significant temperature drift

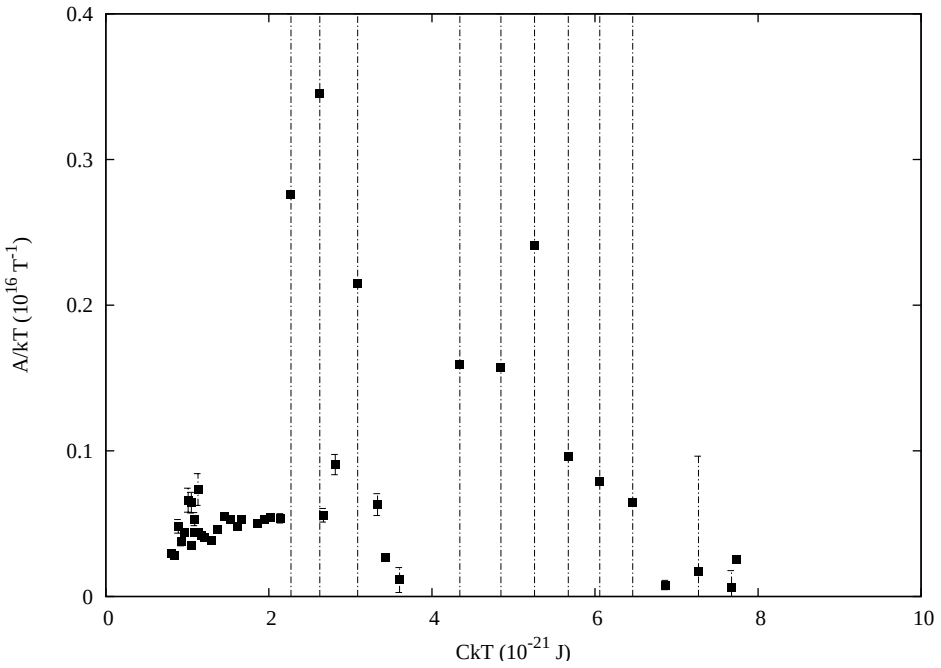

Figure 4.13: *Moment-weighted energy barrier distribution obtained from weak field relaxometry on MR02*

was observed indicates that the sample was in equilibrium at the stated temperature. Any uncertainty here will arise from errors in the calibration of the temperature controls of the SQuID-MPMS.

The material parameters used to analyse the data introduce a significant degree of ambiguity to interpretations of the energy barrier distribution. The fact that magnetite is not a precisely defined substance – ie. the relative proportions of elements in different samples may vary – means that values stated for saturation magnetisation and crystal anisotropy may not apply to the samples used here, and may even differ between these samples. While the values for saturation magnetisation affect only the vertical scaling of results, the anisotropy constant is of particular importance when computing size characteristics from energy barrier data. Ranges of $1.1\text{–}1.4 \times 10^4 \mathrm{J\,m^{-3}}$ have been observed in the literature, so taking the half-width of this as an estimate of the standard error gives a relative error of 24%. Ignoring all other errors, the uncertainty $u(a)$ arising from this is[1]:

$$u(a) = \left|\frac{\partial a}{\partial K}\right| u(K) = \frac{1}{3}\frac{a}{K}u(K)$$

. . . giving a relative error in a of about 8%.

The value of C used to scale the temperature axis in magnetic viscosity analysis relies on the value of τ_0, which is not well known and is difficult to determine experimentally. However, the logarithmic dependence of C on τ_0 means that it is fairly insensitive to changes in this parameter – in fact, the uncertainty in C is actually the uncertainty in the log of τ_0:

$$u(C) = u\left(ln(\tau_0)\right)$$

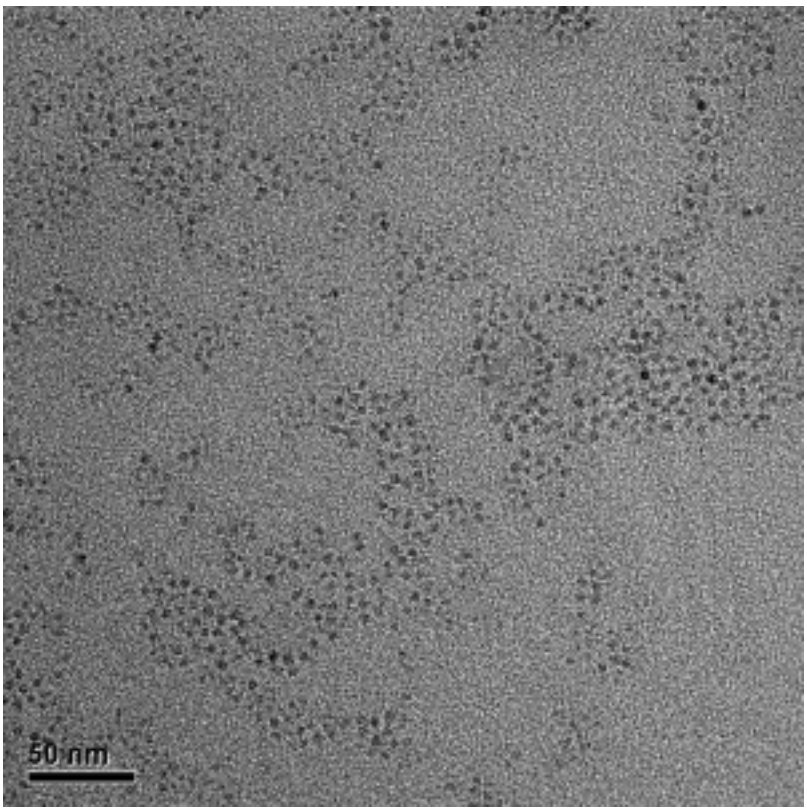

Figure 4.14: *TEM of magnetite nanoparticles taken on the JEOL 3000-FEG. Low contrast, image noise and poor resolution introduce significant uncertainty to measured particle sizes.*

4.2 Transmission Electron Microscopy

Transmission electron micrographs were taken of the same stock solution from which MR02/3 were made. Contrast in the images proved to be a major obstacle to obtaining information from TEM – there is little difference in opacity between 4nm of magnetite and a 40nm carbon film (see Fig. 4.14). Five hundred particles on several images were manually measured, and their distribution is shown in Fig. 4.15.

The particle size distribution obtained from the TEM images is subject to significant uncertainty arising from manual measurement. Selection bias will systematically skew the distribution to larger values, since larger particles are easier to see and are more likely to be counted than smaller particles, and the difficulties in visually resolving the edges of particles in these images introduces further uncertainty to the distribution.

4.3 Small Angle Neutron Scattering

The *Irena* SAS analysis software was used to fit the scattering data obtained from the experiments conducted at AUSANS. Because the contrast in scattering length density between magnetite and the deuterated solvent was quite low, a shell-core model incorporating the oleic acid coating as well as the particle core was employed to fit the data,

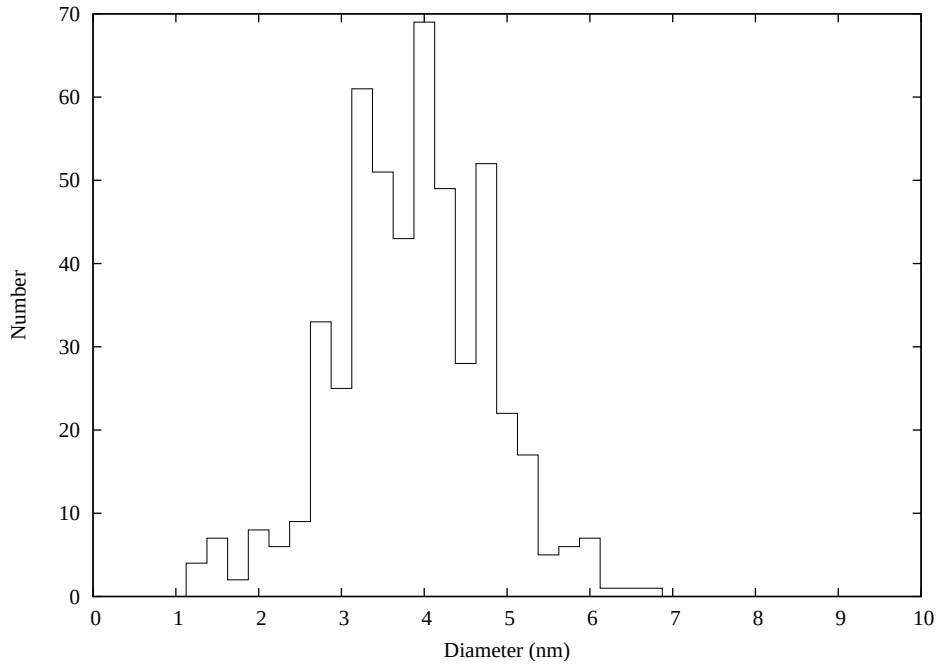

Figure 4.15: *Particle size distribution for MR02 obtained from TEM*

assuming a log-normal distribution for both. The resulting fit gave a particle size distribution mean of 3.2nm and a standard deviation of 0.6nm and is shown in Fig. 4.16.

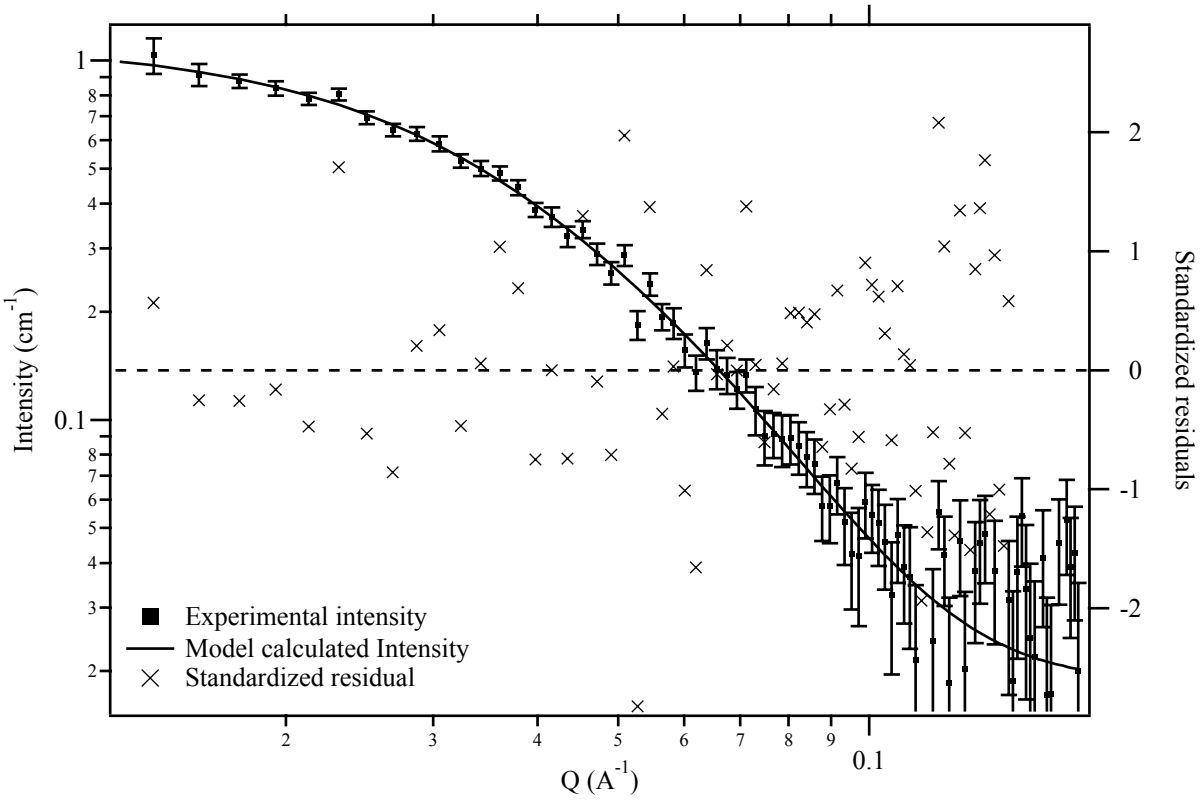

Figure 4.16: *SANS data with fit for MR02 stock redispersed in deuterated cyclohexane, with fit and standardised residuals*

Chapter 5

Comparisons and Conclusions

Of all the magnetometry experiments performed, the information obtained from viscosity experiments appear to give the best picture of the energy barrier distribution and compares favourably with that found by TEM (see Fig. and SANS. However, contributions to the moment-weighted energy barrier distribution that do not originate from the volume distribution of particles can obscure information about particle size and limit the usefulness of this technique. Cooling in a low field appeared to reduce or remove this component allowing the volume distribution to be extracted.

Attempting to separate the particles by suspending them in PDMS had little effect on the anomalous component of the energy barrier distribution. This does not rule out close-range interparticle interactions as the origin of this component, as the particles may have formed aggregates within the suspension.

Of note is the consistency of the magnetometry measurements between the two samples. The viscosity measurements, FC/ZFC measurements and the Langevin fitting all indicated that the mean size of the particles in LH01 was 1.2–1.8 times larger than those in MR02, even though the values for the distributions do vary across the measurement techniques themselves.

Because magnetic viscosity experiments measure the rate of decay of moment $\frac{dm(t)}{d(ln(t))}$, they are very robust against temperature drift in the instrument before the commencement of the measurement. When setting the temperature of the sample chamber, the SQuID-MPMS often overshoots and oscillates about the target temperature – especially at temperatures below 15K, where most of the important detail in the energy barrier distribution occurs for particles with diameters less than 10nm. When this happens before a point is taken in a FC/ZFC measurement the remanent moment is changed irreversibly and the moment measured is no longer meaningful.

Weak field relaxometry also measures the decay rate of the moment, however the experiment relies on the system being close to the equilibrium state and so is sensitive to minor field and temperature fluctuations that may cause the magnetisation to change. Because magnetic viscosity experiments begin with the ensemble in a saturated state – ie. far from equilibrium – this is not an issue.

Method		Size Characteristics					
		MR02			LH01		
		Mean (nm)	Std. Dev. (nm)	Max. (nm)	Mean (nm)	Std. Dev. (nm)	Max.(nm)
TEM		3.7	0.9	6.5			
SANS		3.2	0.6				
FC/ZFC	Blocking Temp			13			19
	EBD	5.5	1.3				
Langevin Fitting		3			4		
Viscosity	70kOe	Large exponential component – could not fit					
	100Oe	Log normal			Log-normal component		
		5.9	1.6	11	11	2.2	17
PDMS		No change from dried sample					
WFR		Unsuccessful					

Table 5.1: *Comparison of methods used to characterise nanoparticle size distribution. The "maximum" of an* a priori *distribution is taken as the 99th percentile.*

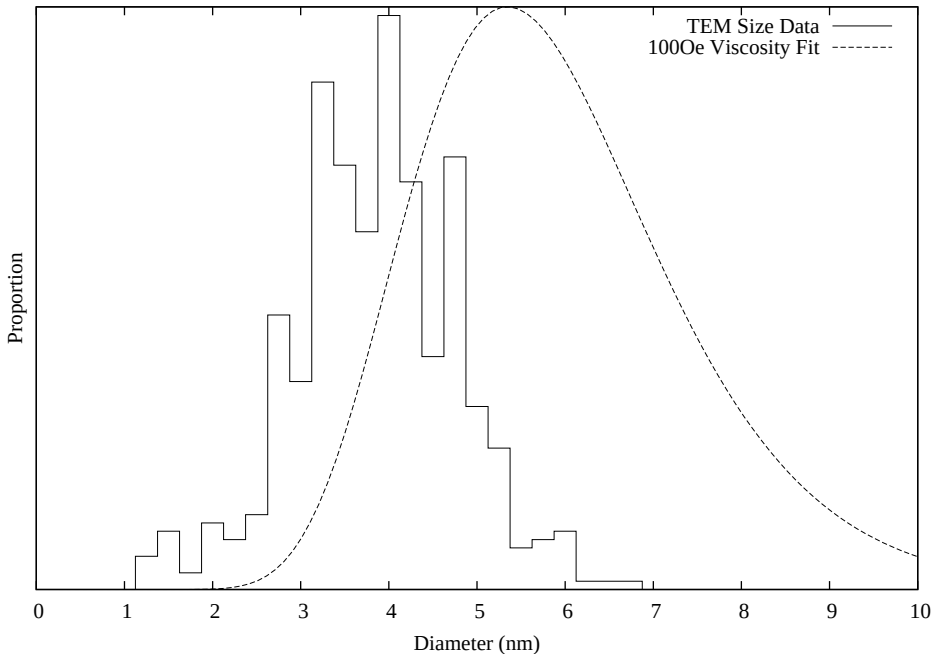

Figure 5.1: *Comparison of particle size distributions for MR02 obtained from TEM and 100Oe viscosity measurements*

The particle sizes found by different techniques are summarised in Tab. 5.1. Though the results compare consistently across the two samples, the values given by each method vary considerably within the samples themselves. The values obtained for the mean particle size in MR02 ranged from 3–6nm, encompassing the values obtained by TEM and SANS. Even though there was no clear agreement across the techniques employed, the outcomes of each experiment helped to construct an overall picture of the strengths and limitations of the various methods.

Appendix A

Relationship Between Energy Barrier and Particle Size Distribution

Presented here is a derivation of the relationship between the energy barrier and volume distribution of particles in an ensemble given in (2.7). Let

$\rho_{E,V}(E)$	be the energy barrier distribution arising from particle volumes
$\rho_V(V)$	be the volume distribution

and assume that the energy barrier of a single particle is due only to its volume – ie. $E \equiv E(V)$. The number of particles with energy barrier less than E is

$$N_E(E) = \int_0^E \rho_{E,V}(E')\, dE'$$

and so by the fundamental theorem of calculus:

$$\begin{array}{rrcl} & \rho_{E,V}(E) & = & \frac{dN_E(E)}{dE} \\ \text{or} & dN_E(E) & = & \rho_{E,V}(E)\, dE \end{array}$$

If we consider the number of particles with volume less than V, similar analysis shows

$$\rho_V(V) = \frac{dN_V(V)}{dV} \tag{A.1}$$

But the volume of a particle is directly related to its energy barrier, and so the particles with volume less than V have energy barriers less than $E(V)$; ie. $N_V(V) \equiv N_E(E(V))$. Using the chain rule on A.1 gives

$$\begin{aligned} \rho_V(V) &= \frac{dN_V(V)}{dV} \equiv \frac{dN_E(E(V))}{d(V)} \\ &= \frac{dN_E(E)}{dE} \cdot \frac{dE(V)}{dV} \end{aligned}$$

$$\Rightarrow \rho_V(V) = \rho_{E,V}(E)\,\frac{dE}{dV}$$

Appendix B

Honours Research Proposal

B.1 Project Title

Characterisation of Magnetic Nanoparticles by Magnetometry Techniques

B.2 Keywords

Magnetic nanoparticles, magnetic viscosity, magnetorelaxometry, magnetic relaxation, weak field magnetorelaxometry

B.3 Supervisors

Dr. Rob Woodward and A. Prof. Tim St. Pierre

B.4 Research Plan

B.4.1 Aims

The project aims to examine how magnetometry measurements on ensembles of magnetic nanoparticles relate to the physical characteristics of the sample, and to compare theoretical models for such experiments. Hysteresis measurements, zero field/field cooled measurements, viscosity and magnetorelaxometry experiments yield information about exchange bias, blocking temperature, presence or absence of different magnetic phases and energy barrier distributions. This information can then, through theoretical models, reveal important characteristics such as the volume distribution of particles in suspension and the stability of particles against oxidisation.

Of particular interest in this thesis will be the relationship between time-dependent magnetorelaxation and the distribution of energy barriers in the system. Two different models for two different experiments have been proposed – one describing magnetorelaxation after the removal of a saturating field[27, 25], and another describing it after removal

of a weak field[6, 23]. No comparisons have been found being done between the models, theoretically or experimentally, and one primary focus of this project is to perform such a comparison.

B.4.2 Significance

Magnetic nanoparticles have a range of uses from production of ferrofluids through to various biomedical applications such as targeted drug delivery, retinal detachment therapy, hyperthermia treatment of tumours and MRI contrast enhancement[22]. For such purposes, knowing the physical characteristics of a sample is necessary for effective use. It is desirable to have particles which are stable against oxidisation, have a narrow range of particle sizes and do not easily aggregate. Oxidisation can manifest as exchange bias, anomalous contributions to the energy barrier distribution, or a drop in the magnetisation per unit volume of the sample. Experiments that determine the distribution of energy barriers in the system can also yield information about the volume distribution and interparticle interactions which may give rise to aggregation.

Current techniques for analysis of nanoparticles other than magnetometry include transmission electron microscopy (TEM) and x-ray diffraction (XRD). TEM gives information about tens or hundreds of particles at most – a very small fraction of the entire sample. Where sample sizes are small and cystallinity poor, XRD is only sensitive to phases comprising greater than 5% of the volume fraction at best. Preparation of samples for TEM and XRD may also change the sample properties.

Magnetometry measurements give information about the entire sample rather than a small number of particles. In order for this information to be useful, however, it must be determined exactly how various magnetometry measurements relate to the properties of the sample.

B.4.3 Methods

Most magnetometry measurements will be made using the superconducting quantum interference device (SQuID) magnetometer. The magnetometry measurements will include 'standard' magnetic measurements such as hysteresis curves above and below the superparamagnetic blocking temperature of the sample and field cooled and zero field cooled measurements. "Viscosity"[27] and weak field relaxometry[6, 23] measurements and models will also be compared.

TEM imaging will be used to look at the size and structure of particles as well as electron energy-loss spectroscopy, energy-filtered TEM and XRD to investigate structure and presence of different phases more thoroughly. Chemical analysis will be used to quantify the elemental content of the samples.

B.4.4 Status

This project is undertaken in the context of the project *Magnetic Nanoparticles for Biomedical Applications* (ARC discovery grant DP0559333). At the time of writing, some magnetometry has been performed on two samples, and TEM analysis started on one.

B.4.5 Problems

Measurements taken with the SQuID may take several days to complete, and problems may arise from this delay. The preparation of samples for TEM, XRD or chemical analysis may require several attempts to produce useful results. The facilities of the Centre for Microscopy and Microanalysis (CMM) must be booked in advance, and this may also cause delays.

B.5 Benefits

Magnetometry offers a different probe into the physical properties of samples of magnetic nanoparticles. Theoretical and experimental investigations of how the magnetic properties relate to other physical properties will allow characterisation of magnetic nanoparticles more thoroughly than that allowed by other methods such as TEM, XRD or chemical analysis. This is of interest from a research perspective and will benefit all areas of application including the manufacturing process of such particles and their biomedical uses.

B.6 Publications

Viscosity in magnetic systems was first discussed by Street[27]. Investigations into the relationship between viscosity measurements and energy barrier distributions have been made by Gorham and others[11, 25] on horse-spleen ferritin. Research into weak field relaxometry has also been looked at – theoretically by Berkov and Kötitz[6] and measurements by Romanus and others[23]. Applications of magnetic nanoparticles in biomedicine have been detailed by Pankhurst and others[22].

B.7 Costs

The cost of subscription to access the CMM facilities is $150 for the year, and is covered by the Faculty of Life and Physical Sciences. The costs incurred by use of the SQuID are for liquid gases and are approximately $120 per day. Initial estimates suggest that the SQuID will be required for a total of 40 days, resulting in a cost of $4800. I estimate that the cost of chemicals used for sample preparation and analysis, and incidental costs will amount to $200. The total cost will be $5000.

B.8 Previous Work

No work was undertaken on this project prior to the 15^{th} of February 2005.

Appendix C

Summary of Student Achievements

From the outset of this project my primary aim was to compare temperature dependent magnetic viscosity[27, 25, 11] and weak field relaxometry[6] as experimental probes of physical properties of magnetic nanoparticles. I began by familiarising myself with the theory behind both techniques and adapting the requirements of weak field relaxometry to our equipment – namely, that a small field be applied for a short time.

Finding suitable experimental parameters for weak field relaxometry proved difficult because of the low moment and the nature of the decay, and because of the constraints of the equipment – the SQuID-MPMS typically takes several minutes to change or remove the applied field, making short magnetising times impractical. I did, however, succeed in confirming the form of the decay given by Berkov and Kötitz even though I was unable to assess whether the information gained from this experiment agreed with that obtained from magnetic viscosity.

I used transmission electron microscopy with the JEOL 2000-F and the JEOL 3000-F and determined that the use of distilled solvents was essential in obtaining useable images, as the small size of the particles limited the contrast and resolution attainable. High resolution TEM was also attempted but was unsuccessful due to polymer contamination of the samples and the small size of the particles.

I travelled to the Bragg Institute at the Australian Nuclear Science and Technology Organisation to perform neutron scattering experiments in order to gain further information about particle size distribution in my samples. I found that the use of protonated solvents introduces problems because of the associated noise from inelastic scattering, and so redispersing the particles in deuterated solvents was necessary to fully exploit this technique.

Ultimately I constructed an overall picture not only of the particle size distributions given by each technique, but of the requirements and limitations of the experiments performed.

Bibliography

[1] *Guide to the Expression of Uncertainty in Measurement*, International Organisation for Standardisation, Switzerland, 1 ed., 1995.

[2] B. Barbara, L. C. Sampaio, A. Marchand, O. Kubo, and H. Takeuchi, *Two-variable scaling of the magnetic viscosity in Ba-ferrite nano-particles*, J. Magn. Magn. Mater., (1994).

[3] G. Beaucage, *Approximations leading to a unified exponential/power-law approach to small-angle scattering*, J. Appl. Cryst., 28 (1995), pp. 717–728.

[4] G. Beaucage, *Small angle scattering from polymeric mass fractals of arbitrary mass-fractal dimension*, J. Appl. Cryst., 29 (1996), pp. 134–146.

[5] G. Beaucage, S. Rane, S. Sukumaran, M. M. Satkowski, L. A. Schechtman, and Y. Doi, *Persistence length of isotactic poly(hydroxy butyrate)*, Macromolecules, 30 (1997), pp. 4158–4162.

[6] D. V. Berkov and R. Kötitz, *Irreversible relaxation behaviour of a general class of magnetic systems*, J. Phys.: Condens. Matter, 8 (1996), pp. 1257–1266.

[7] C. Caizer, *The effect of the external magnetic field on the thermal relaxation of magnetization in systems of aligned nanoparticles*, J. Phys.: Condens. Matter, 17 (2005), pp. 2019–2034.

[8] S. Chikazumi and S. H. Charap, *Physics of Ferromagnetism*, John Wiley and Sons, Inc, 1986.

[9] J. Connolly, T. G. St Pierre, M. Rutnakornpituk, and J. S. Riffle, *Cobalt nanoparticles formed in polysiloxane copolymer micelles: effect of production methods on magnetic properties*, J. Phys. D: Appl. Phys., 37 (2004), pp. 2475–2482.

[10] B. D. Cullity, *Introduction to Magnetic Materials*, Addison-Wesley, 1972.

[11] N. Gorham, *The nature and physical origin of magnetic energy barrier distributions in semi-disordered nanoparticles*, PhD thesis, University of Western Australia, School of Physics, 2005.

[12] M. Hanson, C. Johansson, M. S. Pedersen, and S. Mørup, *The influence of particle size and interactions on the magnetization and susceptibility of nanometre-size particles*, J Phys.: Condens. Matter, 7 (1995), pp. 9269–9277.

[13] L. A. Harris, J. D. Goff, A. Y. Carmichael, J. S. Riffle, J. J. Harburn, T. G. St Pierre, and M. Saunders, *Magnetite nanoparticle dispersions stabilized with triblock copolymers*, Chem. Mater., 15 (2003), pp. 1367–1377.

[14] T. L. Hylton, *Limitations of magnetoresistive sensors based on the giant magnetoresistive effect in granular magnetic composites*, Appl. Phys. Let., 62 (1993), pp. 2431–2433.

[15] R. H. Kodama and A. E. Berkowitz, *Atomic-scale modeling of oxide nanoparticles*, Phys. Rev. B, 59 (1999), pp. 6321–6336.

[16] G. Kostorz, ed., *Neutron Scattering*, vol. 15 of Treatise on Materials Science and Technology, Academic Press, 1979.

[17] A. Labarta, O. Iglesias, L. Balcells, and F. Badia, *Magnetic relaxation in small particle systems: $T\ln(t/\tau_0)$*, Phys. Rev. B, 48 (1993), pp. 10240–10246.

[18] J. J. Lu, H. Y. Deng, and H. L. Huang, *Thermal relaxation of interacting fine magnetic particles – field-cooled and zero-field-cooled magnetisation variation*, J. Magn. Magn. Mater., 209 (2000), pp. 37–41.

[19] A. H. Morrish, *The Physical Principles of Magnetism*, John Wiley and Sons, 1965.

[20] S. Mørup, *Spin-canting and transverse relaxation at surfaces and in the interior of ferrimagnetic particles*, J. Magn. Magn. Mater., 226 (2003), pp. 110–118.

[21] C. B. Murray, C. R. Kagan, and M. G. Bawendi, *Synthesis and characterisation of monodisperse nanocrystals and close-packed nanocrystal assemblies*, Annu. Rev. Mater. Sci., 30 (2000), pp. 545–610.

[22] Q. A. Pankhurst, J. Connolly, S. K. Jones, and J. Dobson, *Applications of magnetic nanoparticles in biomedicine*, J. Phys. D.: Appl. Phys., 36 (2003), pp. R167–R181.

[23] E. Romanus, D. V. Berkov, S. Prass, C. Gross, W. Weitschies, and P. Weber, *Determination of energy barrier distributions of magnetic nanoparticles by temperature dependent magnetorelaxometry*, Nanotechnology, 14 (2003), pp. 1251–1254.

[24] M. Rutnakornpituk, V. V. Baranauskas, J. S. Riffle, J. Connolly, T. G. St Pierre, and J. P. Dailey, *Polysiloxane fluid dispersions of cobalt nanoparticles in silica spheres for use in ophthalmic applications*, European Cells and Materials, 3 (2002), pp. 102–105.

[25] T. G. St Pierre, N. T. Gorham, P. D. Allen, J. L. Costa-Krämer, and K. V. Rao, *Apparent magnetic energy-barrier distribution in horse-spleen ferritin: Evidence for multiple interacting magnetic entities per ferrihydrite nanoparticle*, Phys. Rev. B, 65 (2001).

[26] E. C. Stoner and E. P. Wohlfarth, *A mechanism of magnetic hysteresis in heterogeneous alloys*, Phil. Trans. Roy. Soc., 240 (1948), p. 599.

[27] R. Street and J. C. Woolley, *A study of magnetic viscosity*, Proc. Phys. Soc., Sect. A, 62 (1949), p. 562.

[28] The Australian Nuclear Science and Technology Organisation, *Australian Small Angle Neutron Scattering Facility.* Available online at: http://www.ansto.gov.au/ansto/bragg/hifar/aus.html, 2005.

[29] M. L. Vadala, M. Rutnakornpituk, M. A. Zalich, T. G. St Pierre, and J. S. Riffle, *Block copolysiloxanes and their complexation with cobalt nanoparticles*, Polymer, 45 (2004), pp. 7449–7461.